ANTIOXIDANTS & REDOX SIGNALING
Volume 21, Number 2, 2014

DOI: 10.1089/ars.2013.5690

FORUM ORIGINAL RESEARCH COMMUNICATION

Broad Phenotypic Changes Associated with Gain of Radiation Resistance in Head and Neck Squamous Cell Cancer

Nidhi Bansal,[1,*] Jade Mims,[1,*] Jeffrey G. Kuremsky,[2] Amy L. Olex,[3] Weiling Zhao,[1] Leimiao Yin,[1] Revati Wani,[1] Jiang Qian,[1] Brian Center,[1] Glen S. Marrs,[4] Mercedes Porosnicu,[5] Jacquelyn S. Fetrow,[3] Allen W. Tsang,[1] and Cristina M. Furdui[1]

Abstract

Aims: The central issue of resistance to radiation remains a significant challenge in the treatment of cancer despite improvements in treatment modality and emergence of new therapies. To facilitate the identification of molecular factors that elicit protection against ionizing radiation, we developed a matched model of radiation resistance for head and neck squamous cell cancer (HNSCC) and characterized its properties using quantitative mass spectrometry and complementary assays. ***Results:*** Functional network analysis of proteomics data identified DNA replication and base excision repair, extracellular matrix-receptor interaction, cell cycle, focal adhesion, and regulation of actin cytoskeleton as significantly up- or downregulated networks in resistant (rSCC-61) HNSCC cells. Upregulated proteins in rSCC-61 included a number of cytokeratins, fatty acid synthase, and antioxidant proteins. In addition, the rSCC-61 cells displayed two unexpected features compared with parental radiation-sensitive SCC-61 cells: (i) rSCC-61 had increased sensitivity to Erlotinib, a small-molecule inhibitor of epidermal growth factor receptor; and (ii) there was evidence of mesenchymal-to-epithelial transition in rSCC-61, confirmed by the expression of protein markers and functional assays (*e.g.,* Vimentin, migration). ***Innovation:*** The matched model of radiation resistance presented here shows that multiple signaling and metabolic pathways converge to produce the rSCC-61 phenotype, and this points to the function of the antioxidant system as a major regulator of resistance to ionizing radiation in rSCC-61, a phenomenon further confirmed by analysis of HNSCC tumor samples. ***Conclusion:*** The rSCC-61/SCC-61 model provides the opportunity for future investigations of the redox-regulated mechanisms of response to combined radiation and Erlotinib in a preclinical setting. *Antioxid. Redox Signal.* 21, 221–236.

Introduction

HEAD AND NECK SQUAMOUS CELL CANCER (HNSCC) is the eighth most common cause of cancer death worldwide, and it accounts for 3% to 4% of cancers in the United States (26). The treatment options available for HNSCC patients rely primarily on various combinations of surgery, radiation, and chemotherapy, depending on the stage and resectability of the disease. Many patients are, however, medically unfit for surgery or have unresectable tumors because of the disease extent or involvement of critical structures. To alleviate the substantial toxicity associated with the combined radiation and chemotherapy regimens that are often prescribed for these patients, the focus has shifted recently toward the use of targeted agents alone or in combination with surgery, radiation, or chemotherapy. Epidermal growth factor receptor (EGFR) constitutes an attractive target for the treatment of HNSCC for a number of reasons: (i) EGFR protein is increased in >80% of HNSCC tumors (8); (ii) Cetuximab, a monoclonal antibody against EGFR, was shown to improve the response to radiation in patients with locally advanced HNSCC and is currently

[1]Section on Molecular Medicine, Department of Internal Medicine, Wake Forest School of Medicine, Winston-Salem, North Carolina.
[2]Department of Radiation Oncology, Wake Forest School of Medicine, Winston-Salem, North Carolina.
Departments of [3]Computer Science and [4]Biology, Wake Forest University, Winston-Salem, North Carolina.
[5]Section of Hematology and Oncology, Department of Internal Medicine, Wake Forest School of Medicine, Winston-Salem, North Carolina.
*Authors contributed equally to this work.

Innovation

The results of this study point to the complexity and interdependence of the mechanisms employed by radiation-resistant cells to withstand and repair the damage induced by radiation at the center of which stands the regulation of reactive oxygen species by the antioxidant system. The matched model of radiation resistance for head and neck cancer discussed here provides a valuable opportunity to investigate the molecular mechanisms of response to combined radiation and Erlotinib in a preclinical setting.

approved for clinical use (9); and (iii) there are a number of small-molecule inhibitors against EGFR that have shown clinical success for the treatment of a number of cancers. Erlotinib (Tarceva) is one such small-molecule EGFR inhibitor currently in clinical trials for the treatment of HNSCC and nonsmall cell lung cancer. The goal of the studies presented here was to establish a clinically relevant *in vitro* model of resistance to radiation that would enable us to investigate the mechanisms contributing to radiation resistance, the response to Erlotinib, and the interconnecting networks which may regulate the response to radiation with the use of targeted agents.

Most reported studies investigating the resistance to radiation involve a comparative analysis of cancer cell lines established from patients with distinct genetic backgrounds and complex medical and treatment histories (32). A better understanding of resistance to radiation can be achieved by investigating the molecular and cellular features that characterize a clonal population which is resistant to radiation in matched cell lines. In this study, we generated a radiation-resistant head and neck cancer cell line (rSCC-61) from the radiation-sensitive SCC-61 cell line by fractionated radiation. We characterized the two cell lines in terms of their proteomic composition, survival in response to radiation and Erlotinib treatment, metabolic features, and a number of other parameters to unveil the mechanisms of resistance to radiation and response to Erlotinib in HNSCC. The most unexpected findings of our studies were the increased sensitivity to Erlotinib and the emergence of epithelial phenotype in rSCC-61 cells relative to the parental SCC-61 cells, which were Erlotinib resistant and had mesenchymal properties. This is significant in the context of recent studies showing the presence of both mesenchymal and epithelial cells in tumors of advanced-stage HNSCC (5, 39).

Thus, the findings presented here have profound clinical implications for identifying molecular markers of radiation resistance that are associated with epithelial cell types in HNSCC and may offer selective avenues for drug targeting of epithelial radiation-resistant HNSCC cells in tumors.

Results

Generation of a matched model of radiation resistance for HNSCC and its primary characterization

The radiation-sensitive SCC-61 cells previously derived from an HNSCC tumor located at the base of the tongue (52) were treated *in vitro* with fractionated radiation (2 Gy) for a cumulative total of 16 Gy. The resulting cell population was plated at a low density on soft agar, and eight single-cell-derived colonies were picked and expanded in culture. The clone R8E, hereafter called rSCC-61, was randomly selected for further investigation.

Cell morphology. The first noted difference between the SCC-61 and the rSCC-61 cells was their morphology. The SCC-61 cells were round and larger in size, while the rSCC-61 were spindle shaped and smaller. To quantify the change in morphology, we calculated the nucleus-to-cytoplasm ratio (NCR) using imaging analysis (Fig. 1A). The results show an approximately twofold higher NCR in rSCC-61 (1.1 ± 0.05) compared with SCC-61 (0.5 ± 0.01) (Fig. 1B). A potential explanation for the increased NCR in rSCC-61 is provided by the quantitative proteomics analysis below, indicating the downregulation of proteins involved in cytoskeletal organization in rSCC-61.

Response to radiation treatment. Clonogenic assays were performed to determine the radiation response parameters for the SCC-61 and rSCC-61 cells (Fig. 1C and Supplementary Table S1; Supplementary Data are available online at www.liebertpub.com/ars). The D_0 values for rSCC-61 and SCC-61 were 2.04 and 1.3, respectively, confirming the acquisition of a radiation-resistant phenotype in rSCC-61. The results for rSCC-61 are comparable with other HNSCC cell lines that are isolated from radiation-resistant tumors (46, 51).

Cell cycle analysis. Cell cycle analysis was performed at 24 h after treatment with ionizing radiation. In the absence of radiation, the SCC-61 and rSCC-61 cells showed a similar distribution of cells in the G1, S, and G2/M phases of the cell cycle (*e.g.,* rSCC-61 $51.0\% \pm 5.2\%$, $34.1\% \pm 0.1\%$, and $14.9\% \pm 5.3\%$, respectively) (Fig. 1D). Treatment with 2 Gy radiation induced increased G2/M arrest in SCC-61 cells ($45\% \pm 15.4\%$) compared with rSCC-61 ($22.9\% \pm 8.9\%$).

Response to Erlotinib treatment. The resistance to Erlotinib treatment of SCC-61 cells has been previously reported (30, 45). To determine whether the acquired resistance to radiation in rSCC-61 has affected the response to Erlotinib, cell viability assays were performed at increasing concentrations of Erlotinib (0.5 to 100 μM). The IC50 for rSCC-61 was $4.5 \pm 0.4\ \mu M$ compared with $> 50\ \mu M$ for SCC-61, suggesting a more than 10-fold increase in sensitivity to Erlotinib in rSCC-61 (Fig. 1E). Tumors become resistant to targeted inhibitors of EGFR through diverse mechanisms, which include acquisition of oncogenic mutations (*e.g.,* mutations that inhibit the binding of inhibitors to EGFR but do not decrease its kinase activity), activation of bypass pathways, epithelial-to-mesenchymal transformation (EMT), and others [reviewed in Ref. (13)]. Here, we first explored the status of EGFR and Akt expression and activation, as reports have correlated increased activation of EGFR/Akt with resistance to EGFR inhibitors (11, 19). The phosphorylation status of EGFR and its downstream signaling molecule Akt in SCC-61 and rSCC-61 cells was monitored using Western blot analysis. The results show a decrease in EGFR signaling in rSCC-61 cells by $\sim 50\%$ despite an overall increase in tyrosine phosphorylation in rSCC-61 (Fig. 1F). The difference in EGFR phosphorylation is consistent with the response to

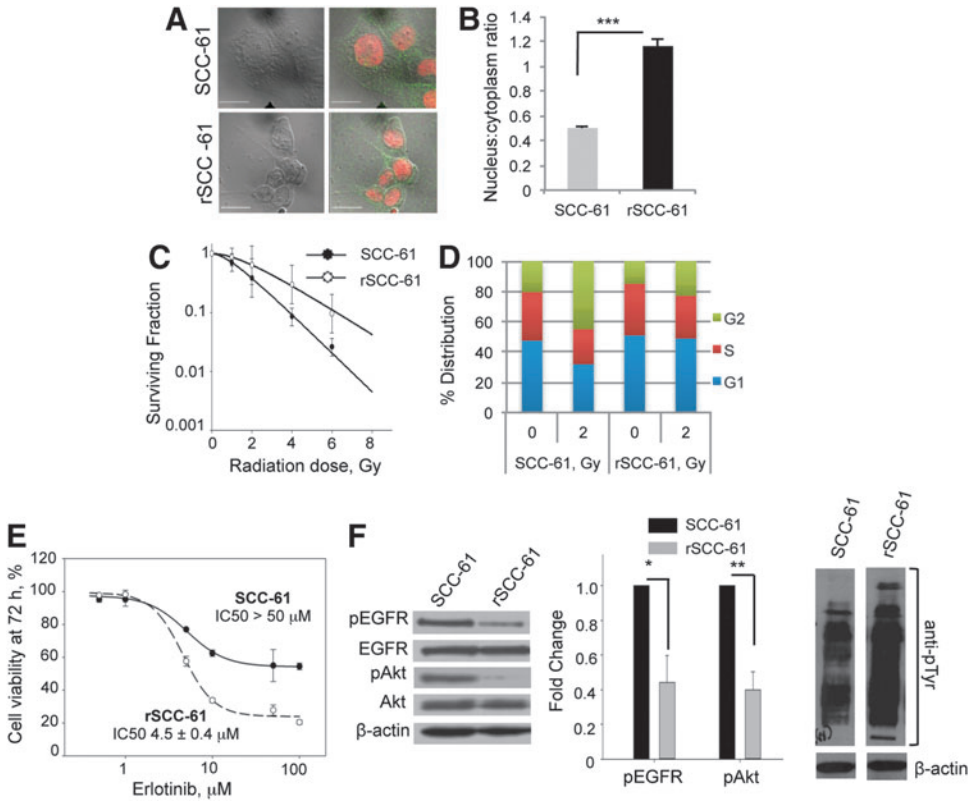

FIG. 1. rSCC-61 exhibits increased resistance to radiation and increased sensitivity to Erlotinib in comparison to SCC-61. **(A)** Cell morphology. The SCC-61 and rSCC-61 cells were immunostained with anti-EGFR antibodies, and the nucleus was stained with Topro-3-iodide to mark the cell and nuclear boundaries, respectively. Images were acquired using the Zeiss LSM510 confocal microscope. The scale bars represent a distance of 20 μm. **(B)** Quantification of nucleus-to-cytoplasm ratio (NCR). The NCR was quantitated using ImageJ software from confocal images shown in panel **A** (*** $p < 0.001$, $n = 50$ cells). **(C)** Clonogenic assay to determine the response to radiation. The survival curves of SCC-61 and rSCC-61 cells are shown in response to increasing doses of radiation. Data were fit to multi-target and linear-quadratic models. The values of D_0, α and β parameters are listed in Supplementary Table S1. **(D)** Cell-cycle analysis. The percent distribution of SCC-61 and rSCC-61 cells in the G1, S, and G2 phases of the cell cycle was determined at 24 h after treatment with the 0 and 2 Gy radiation doses. **(E)** Cell viability in response to Erlotinib treatment. MTT assay was used to measure cell viability at 72 h post-treatment with Erlotinib (0, 0.5, 1.0, 10.0, 25.0, 50.0, and 100.0 μM). The percentage of viable cells was calculated relative to the untreated control. **(F)** Western blot analysis of EGFR and Akt phosphorylation. SCC-61 and rSCC-61 cell lysates were immunoblotted with antibodies against pEGFR, total EGFR, pAkt, total Akt, total pTyr, and β-actin and quantified using ImageJ (pEGFR: * $p = 0.022$, $n = 3$; pAkt: ** $p = 0.004$, $n = 3$). EGFR, epidermal growth factor receptor; MTT, 3-(4,5-dimethylthiazol-2-yl)-2,5-diphenyltetrazolium bromide.

Erlotinib and literature cited earlier. In addition to EGFR phosphorylation, the response to Erlotinib has also been linked to the regulation of integrin expression (27), lipid rafts content (25), and EMT (16). The results described next for the SCC-61/rSCC-61 system are consistent with all these independent studies. The finding of acquired sensitivity to Erlotinib further increases the value of the SCC-61/rSCC-61 cell model that now enables the investigation of the mechanisms of response to Erlotinib in the background of a matched radiation-resistant and radiation-sensitive cell model. It also points to the importance of pursuing clinical trials to investigate the treatment of head and neck tumors with Erlotinib, as tumors that are resistant to radiation may respond to Erlotinib treatment.

Quantitative proteomic analysis of SCC-61 and rSCC-61

To identify the underlying molecular mechanisms of the acquired resistance to radiation in rSCC-61, a quantitative proteomics analysis of SCC-61 and rSCC-61 was performed using stable isotope labeling with amino acids in cell culture (SILAC) and mass spectrometry. The experimental design is summarized in Figure 2A. The SCC-61 and rSCC-61 cells were cultured in medium containing light (SCC-61) and heavy (rSCC-61) isotopes of lysine and arginine. The SCC-61 and rSCC-61 lysates were then normalized with regard to their protein concentration, combined in a 1:1 ratio, and analyzed using a Thermo LTQ Orbitrap mass spectrometer. The data were processed using the Proteome Discoverer 1.2 (Thermo Fisher Scientific) and searched against the UniProtKB human database. The results were filtered using a false discovery rate of 1%, which yielded quantitative data for 965 proteins. Data in Figure 2B show the distribution of protein ratios in rSCC-61 *versus* SCC-61 (heavy/light) for 920 proteins whose ratios range from 0.017 to 50.5. The remaining 45 proteins listed in Supplementary Table S2 had a ratio of less than 0.01, with the lower limit set in our

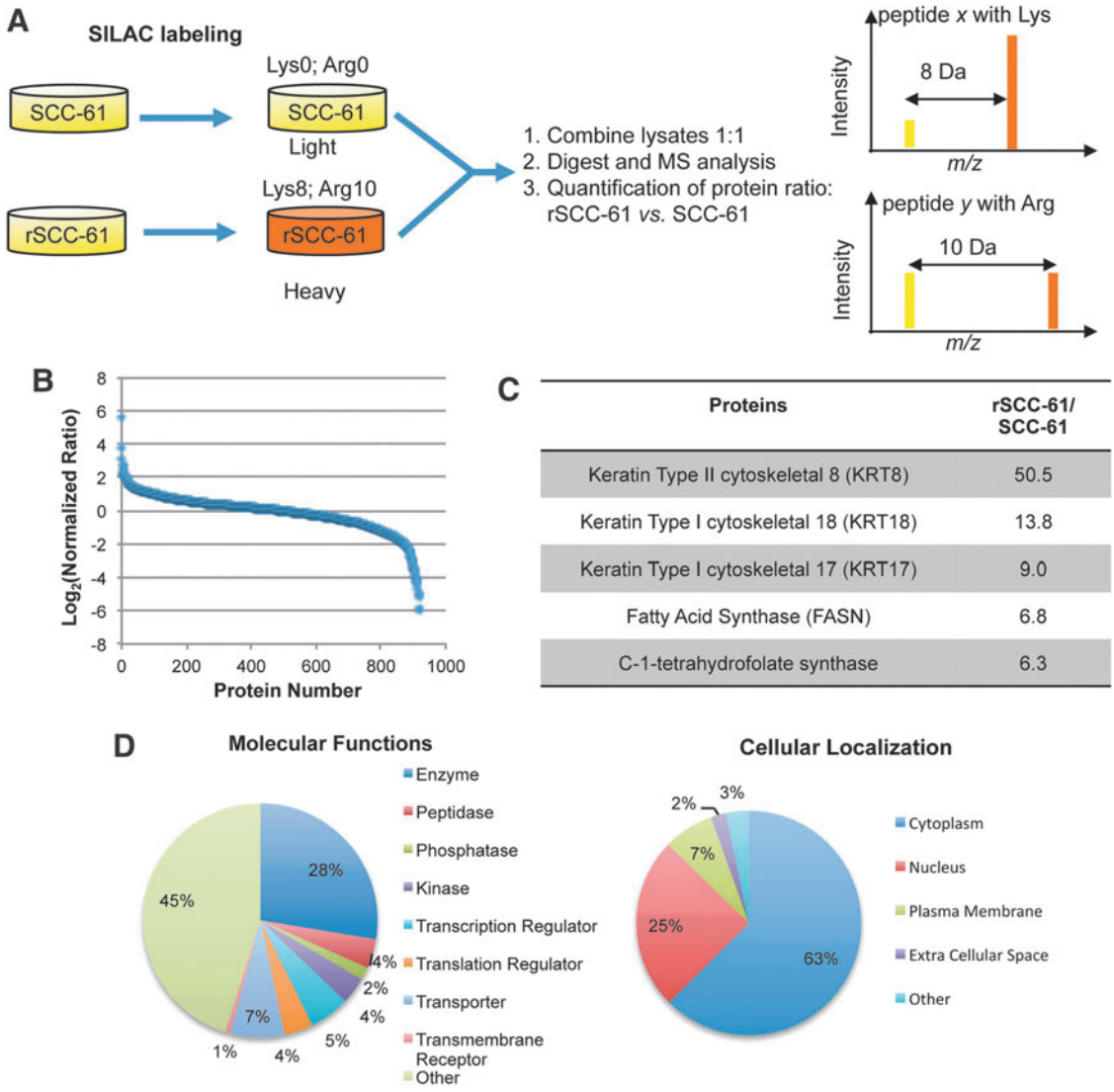

FIG. 2. Summary of quantitative proteomic analysis of SCC-61 and rSCC-61. (A) Schematic representation of mass spectrometry-based comparative proteomics approach. SCC-61 and rSCC-61 were cultured in media containing light and heavy isotopes of Lys and Arg as described in the ''Materials and Methods'' section. The normalized mixture of SCC-61 and rSCC-61 proteins lysates was analyzed by mass spectrometry. **(B)** Protein ratios in rSCC-61 *versus* SCC-61 (heavy/light). The data were normalized to the median protein ratio. Approximately 30% of the proteins identified had altered protein status in rSCC-61 relative to SCC-61. **(C)** List of the top upregulated proteins in rSCC-61. The protein ratios generated by the SILAC proteomics analysis were arranged in descending order. An extended list is included in Supplementary Table S3. **(D)** Cellular localization and functions of the proteins identified in the proteomic analysis. The list of 920 proteins with ratios between 0.017 and 50.5 was input into the IPA. The pie charts represent the classification of the proteins based on their cellular localization or functions. The pie charts corresponding to the entire 965 proteins dataset is included in Supplementary Figure S1. IPA, Ingenuity Pathway Analysis; SILAC, stable isotope labeling with amino acids in cell culture. To see this illustration in color, the reader is referred to the web version of this article at www.liebertpub.com/ars

quantitation algorithm. These are proteins that are more than 100-fold downregulated in rSCC-61 and were considered separately in an effort to avoid bias in the downstream computational analysis. Ingenuity Pathway Analysis (IPA) was used to analyze the 920 and 45 proteins datasets (i) to determine the distribution of subcellular locations and protein functions, and (ii) to identify biological networks and molecular functions that are enriched in proteins significantly which are up- or downregulated in rSCC-61.

Overall, the most upregulated proteins in rSCC-61 were keratins (>8-fold upregulation) followed by a 6.8-fold increase in the fatty acid synthase (FASN) (Fig. 2C) and a number of other proteins such as the deoxyuridine 5′-triphosphate nucleotidohydrolase (DUT), peroxiredoxins (PRX), and GSK3β with a potential function in mediating the resistance to radiation in rSCC-61 (an extended list is included in Supplementary Table S3) [*e.g.,* GSK3β (33); FASN (29); PRX (41)].

The distribution of subcellular locations and functions of the 920 proteins is shown in Figure 2D. The IPA core analysis of this dataset identified that among proteins which were downregulated in rSCC-61 cells, there was significant enrichment of proteins involved in cell death ($p<0.001$; z score: -1.174)

and apoptosis ($p < 0.001$; z score: -2.016) (Supplementary Table S4). Similarly, the IPA analysis of the 45 protein dataset indicated a decrease in cell death ($p < 0.001$), a decrease in cell migration ($p < 0.001$; z score: -2.354), and downregulation of EGF signaling in rSCC-61 ($p < 0.001$; z score: -2.574). These results are consistent with the increased survival of rSCC-61 in response to radiation and the anti-proliferative effect of Erlotinib in rSCC-61. Interestingly, 36% (16 proteins) of the 45 downregulated proteins are localized in the extracellular space (Supplementary Fig. S1). Among these, integrin alpha 6, thrombospondin 1, and vitronectin are required for the regulation of focal adhesion and extracellular matrix (ECM)-receptor interactions.

Mapping of proteomics data to KEGG and HPRD human interaction networks and functional analysis

Cytoscape version 2.8.2 (47) was used to mine and visualize interactions present in the 920-protein dataset as described in the ''Materials and Methods'' section. Two interaction databases—the Kyoto Encyclopedia of Genes and Genomes (KEGG) (28) and the Human Protein Reference Database (HPRD) (43)—were used in the analysis. The KEGG database contains known canonical pathway interactions, while HPRD comprises known protein–protein interactions derived from experimental data, thus providing overlapping as well as distinct information. In order to identify which parts of these networks contained significantly altered proteins in rSCC-61 cells, all proteins with an absolute fold change of 2.0 or greater were extracted, along with first neighbors and all associated interactions, to create the KEGG interaction subnetwork containing 130 nodes and 264 interactions (Supplementary Fig. S2) and the HPRD interaction subnetwork containing 184 nodes and 141 interactions (Fig. 3). Annotation analysis was performed on the lists of UniProt accessions representing the proteins present in the KEGG (130 proteins) and HPRD (184 proteins) networks using the tools provided by the Database for Annotation, Visualization, and Integrated Discovery (DAVID) (23, 24). A number of significantly regulated canonical pathways ($p < 0.05$) in rSCC-61 cells were identified by these analyses: DNA replication and base excision repair, ECM-receptor

KEGG pathway	P value
DNA Replication	0.004
ECM-receptor Interaction	0.017
Base Excision Repair	0.025
Cell Cycle	0.025
Focal Adhesion	0.028

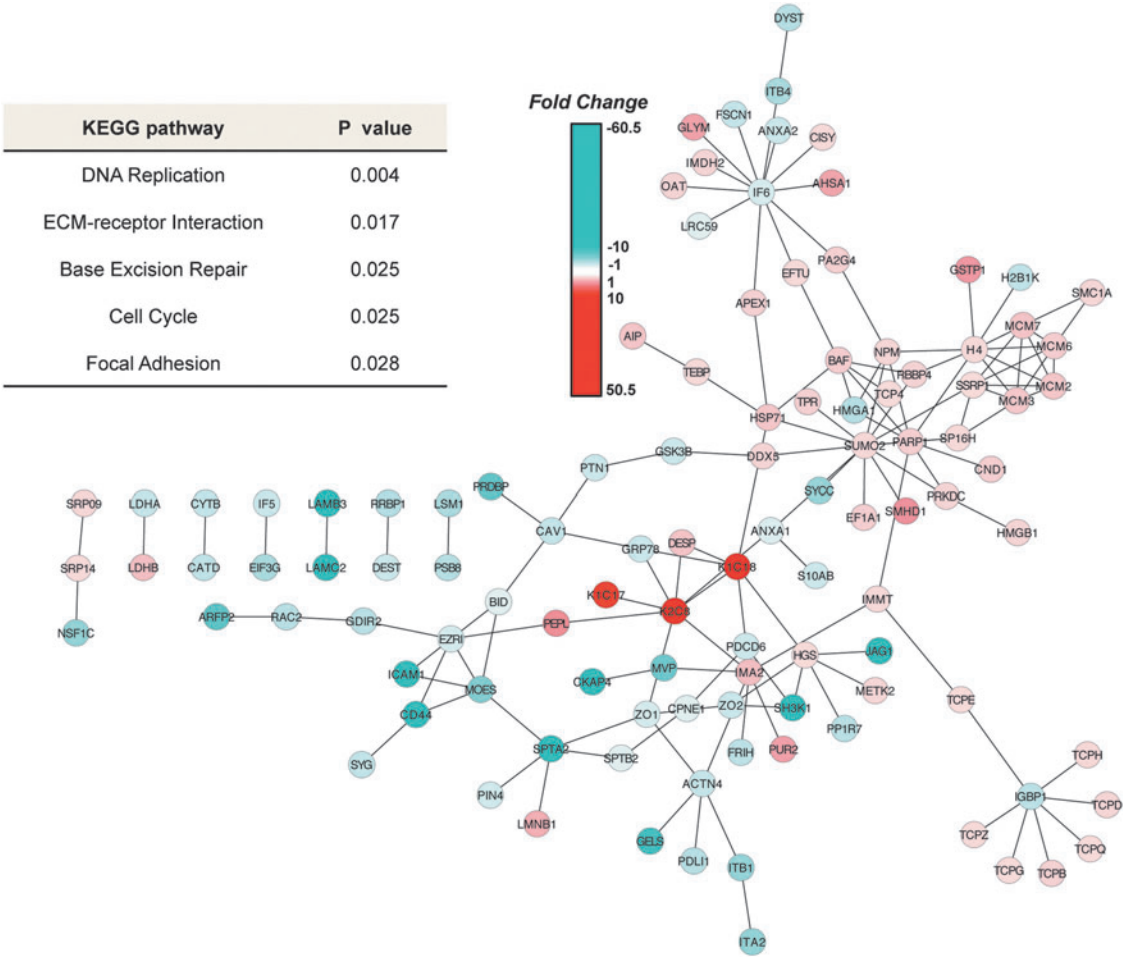

FIG. 3. Functional network analysis—Human Protein Reference Database (HPRD) interaction subnetwork. HPRD was used in Cytoscape version 2.8.2 to create a subnetwork consisting of significantly regulated nodes (≥ 2.0 or ≤ -2.0-fold change). Node colors represent fold change, where red is upregulation and blue is downregulation as indicated by the color bar. DAVID analysis of the Uniprot IDs of these significantly regulated nodes identified 5 significantly over-represented ($p < 0.05$) pathways in this network, which are listed in the table on the left. DAVID, Database for Annotation, Visualization and Integrated Discovery. To see this illustration in color, the reader is referred to the web version of this article at www.liebertpub.com/ars

interaction, cell cycle, focal adhesion, and regulation of actin cytoskeleton (Fig. 3 and Supplementary Table S5A–E). Complementary data to support these results and the significance of the findings to the radiation-resistant phenotype of rSCC-61 are presented in the next few sections.

Mesenchymal-to-epithelial transition in rSCC-61

Functional annotation of the KEGG and HPRD networks identified proteins involved in the regulation of actin cytoskeleton, focal adhesion, and ECM-receptor interaction ($p < 0.05$) in rSCC-61 to be significantly downregulated. Combined with the noted morphological differences between SCC-61 and rSCC-61 cells, and the observation that proteins such as keratins (KRT8, KRT18) and periplakin are upregulated in rSCC-61, these events point to a mesenchymal-to-epithelial transition in rSCC-61. To further confirm the epithelial phenotype in rSCC-61, we performed semi-quantitative PCR and Western blot analysis to evaluate the expression of traditional markers of mesenchymal-to-epithelial transition: E-cadherin and vimentin. In comparison to SCC-61, the rSCC-61 cells displayed a higher expression of E-cadherin and a lower expression of vimentin, which was further confirmed by Western blot analysis (Fig. 4A). Another hallmark that differentiates between mesenchymal and epithelial cells is their migration properties. From the proteomics analysis, it was evident that rSCC-61 exhibits reduced ECM-receptor interaction and focal adhesion, which are known mediators of migration (relative change of integrins and other proteins mapping to the ECM-receptor interaction and focal adhesion networks is shown in Fig. 4B and Supplementary Tables S5D and S5E) (48, 49). A trans-well migration assay was performed and confirmed the significantly lower migration of rSCC-61 relative to the SCC-61 cells ($p < 0.001$; Fig. 4C). Cumulatively, these results point to a transition from mesenchymal phenotype in SCC-61 toward an epithelial phenotype in rSCC-61.

Measurement of intracellular and extracellular lactic acid

Lactic acid has been reported as one of the metabolic factors affecting migration (21). The proteomics data showed downregulation of lactate dehydrogenase A (LDH-A, threefold) and upregulation of lactate dehydrogenase-B (LDH-B, threefold) in rSCC-61, suggesting a shift from glucose routing into lactic acid synthesis in SCC-61 to pyruvate in rSCC-61 (Fig. 5A). To determine the intracellular and extracellular lactic acid in rSCC-61 and SCC-61 cells during cell growth, the lactic acid assay was performed as described in the ''Supplementary Materials and Methods'' section. Significantly higher levels of both intracellular and extracellular lactate were observed in SCC-61 cells at 48 and 72 h of cell growth (Fig. 5B, C). Extracellular pH of the two cell lines was also monitored at 4, 8, 24, 48, and 72 h after cell seeding, and the results show increased acidification of the extracellular environment in SCC-61 culture compared with rSCC-61 (Fig. 5D). Both the efflux of lactate and H^+-ions from inside the cell to the extracellular medium are likely contributing to the pH change (42). The mechanism of this dynamic process is not completely understood, and we will be investigating other potential sources that could lead to the observed differences in media acidification between the SCC-61 and rSCC-61 cells.

Reactive oxygen species, the antioxidant system, and DNA damage in SCC-61 and rSCC-61 cells

Under normal conditions, physiological levels of reactive oxygen species (ROS) are under the tight control of the cellular antioxidant system, which is considered responsible for maintaining ROS below the threshold at which DNA damage can occur while enabling temporal and localized accumulation of these species when needed during cell growth. Cancer cells, however, are known to accumulate intracellular ROS,

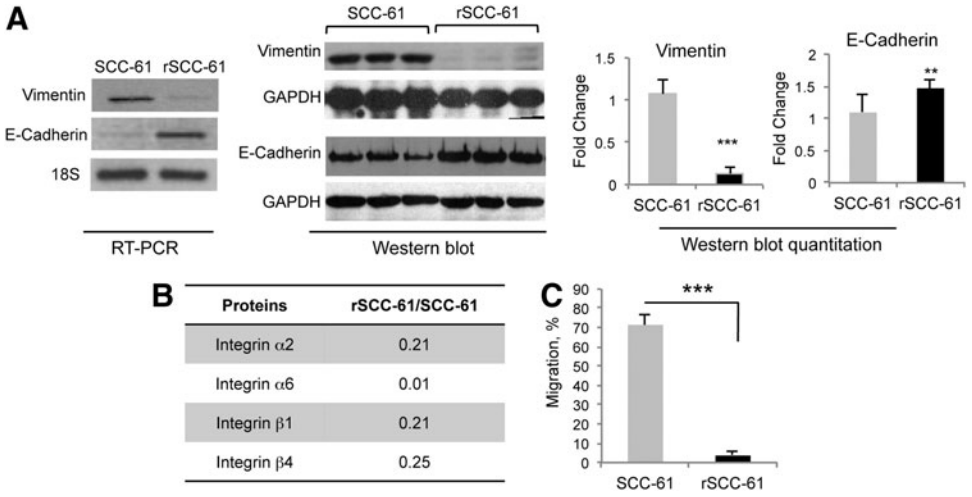

Proteins	rSCC-61/SCC-61
Integrin α2	0.21
Integrin α6	0.01
Integrin β1	0.21
Integrin β4	0.25

FIG. 4. rSCC-61 cells are associated with mesenchymal-to-epithelial transition (MET). (A) Semi-quantitative PCR and Western blot analysis of Vimentin and E-cadherin. The relative expression of vimentin and E-cadherin in SCC-61 and rSCC-61 was determined using semi-quantitative PCR ($n = 1$). 18S RNA amplification was used as endogenous control. Three out of five biological replicates are shown for the Western blot analysis; quantification is based on all five replicates and taking into account the differences in GAPDH (Vimentin: $^{***}p < 0.001$, $n = 5$; E-cadherin: $^{**}p = 0.01$, $n = 5$). **(B)** Table showing the protein ratio of integrin isoforms identified by the SILAC proteomics analysis. **(C)** Trans-well migration assay. The migration properties of SCC-61 and rSCC-61 cells were quantified using the trans-well migration assay described in the ''Supplementary Materials and Methods'' section ($^{***}p < 0.001$, $n = 3$).

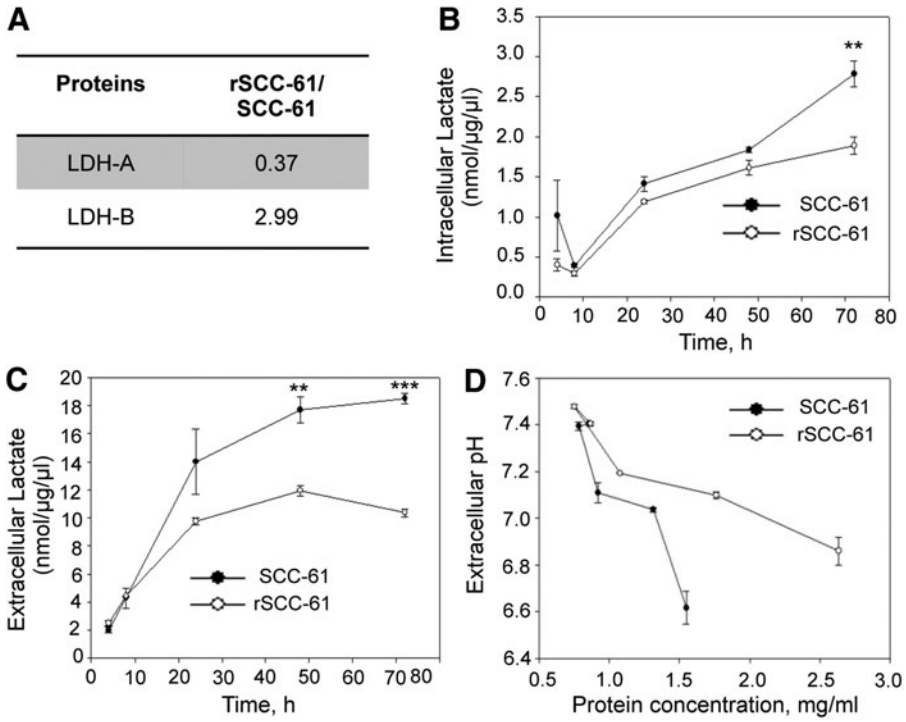

FIG. 5. The stoichiometry of LDH-A and LDH-B determines the pyruvate/lactate equilibrium. **(A)** Table showing the ratios of LDH-A and LDH-B in rSCC-61 and SCC-61 determined by the SILAC proteomic analysis. **(B, C)** Intracellular and extracellular lactate measurements. SCC-61 and rSCC-61 were harvested at different time intervals after seeding (4, 8, 24, 48, and 72 h). Total protein concentrations were estimated for each time point. The intracellular lactate levels were estimated and plotted against the respective time points **(B)** (72 h: $**p = 0.01$, $n = 3$). Similarly, the extracellular lactate levels were estimated from the culture medium collected at each of the respective time points **(C)** (48 h: $**p = 0.005$, $n = 3$; 72 h: $***p = 0.001$, $n = 3$). **(D)** A decrease in extracellular pH with cell growth. The extracellular pH of the SCC-61 and rSCC-61 cells in culture was measured at 4, 8, 24, 48, and 72 h after seeding the cells. Protein concentration at each time point was measured and plotted on the x-axis. LDH-A, lactate dehydrogenase A.

and numerous studies have linked ROS in cancer cells to processes such as DNA damage, response to therapies, cellular plasticity, and others (18). The proteomics analysis described here revealed the upregulation of a number of antioxidant proteins in rSCC-61 (Supplementary Table S6). The upregulation of proteins such as glutathione S-transferase pi (GSTpi) and PRX was also previously reported in a comparison study of the radiation-resistant AMC-HN9 and the radiation-sensitive AMC-HN3 head and neck cancer cell lines (32). Thus, one of our first goals was to assess the intracellular ROS in the SCC-61 and rSCC-61 cells and to validate the upregulation of antioxidant proteins. The dichlorofluorescein (DCF) staining and imaging analysis showed lower ROS in rSCC-61 compared with SCC-61 (Fig. 6A). Western blot analysis showed increased levels of antioxidant proteins such as Prx1, Prx 2, and GSTpi, thus further corroborating the proteomic findings (Fig. 6B). In addition, the higher ratio of superoxide dismutase (SOD) to catalase in SCC-61 offered reasoning for the higher ROS accumulation in SCC-61. We have further monitored the hyperoxidation of Prx proteins (Prx-$SO_{2/3,}$ markers of oxidative stress) and PTEN expression and oxidation. PTEN is a known negative regulator of Akt and to be consistent with the pAkt results in Figure 1F, we posed that PTEN oxidation would be lower in rSCC-61 as a result of lower ROS and/or there would be increased expression of PTEN in rSCC-61. The analysis in Figure 6B shows a higher expression of PTEN in rSCC-61, thus confirming a part of our hypothesis. Due to the difference in protein expression, we could not reliably conclude whether there is a shift in protein migration (oxidized PTEN migrates slightly lower than the reduced protein). However, given the lower ROS in rSCC-61, it is unreasonable to hypothesize higher PTEN oxidation in this cell line. Taking this together with increased expression of PTEN in rSCC-61, the results clearly point to combined EGFR and PTEN-mediated downregulation of Akt activity. The contribution of ROS to EGFR/Akt signaling will be further investigated in future using complementary approaches.

Glutathione is another component of the antioxidant system that is implicated in the response to radiation (10, 37). We quantified total, oxidized, and reduced glutathione using the glutathione assay kit as described in the ''Supplementary Materials and Methods'' section. While the total glutathione was significantly less in rSCC-61 than in SCC-61, the endogenous reduced glutathione was significantly higher in rSCC-61 (Fig. 6C). Nevertheless, the majority of glutathione resided in oxidized state in both cell lines, suggesting a lesser redox buffering capacity by this system in response to an ROS challenge.

To determine whether the combined effects of increased ROS scavenging capacity in rSCC-61, and the upregulation of proteins involved in DNA replication and base-excision repair result in lesser radiation-induced DNA damage, we monitored the γH2AX protein, a known marker of DNA

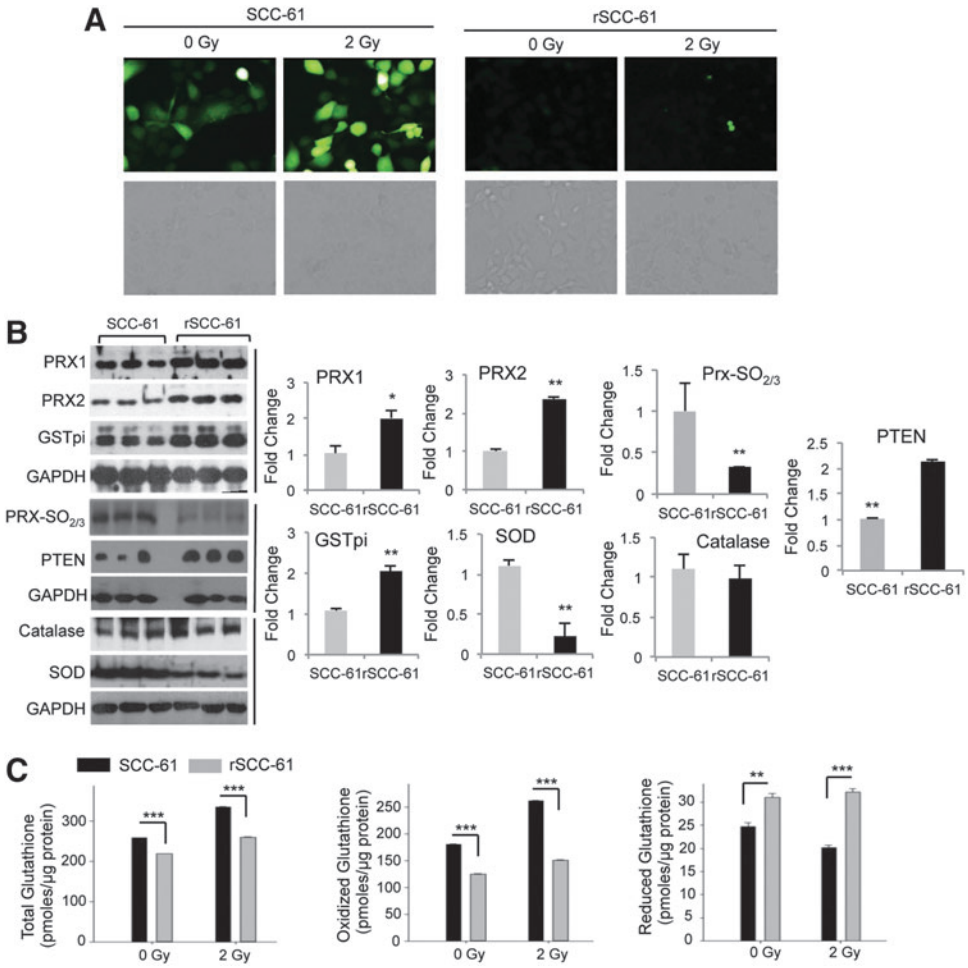

FIG. 6. rSCC-61 have decreased ROS and reduced DNA damage. (A) ROS imaging analysis. DCF fluorescence images of ROS in SCC-61 and rSCC-61 cells before and after treatment with radiation (control −0 Gy and 2 Gy). Images were captured using the Arcturus PixCell II laser capture microscope under 20× objective. **(B)** Western blot analysis of proteins involved in the antioxidant system in rSCC-61 and SCC-61. Three out of five biological replicates are shown here for Prx1 and 2, Prx-SO2/3, PTEN, GSTpi, SOD, and catalase. Quantification is based on all five replicates ($n=5$) and taking into account the differences in GAPDH (Prx1: $*p=0.03$; Prx2: $**p=0.003$; Prx-$SO_{2/3}$: $**p=0.0012$; GSTpi: $**p=0.0014$; SOD: $**p=0.004$; Catalase: $p>0.05$; PTEN: $**p=0.009$). **(C)** Quantification of glutathione. Glutathione (total, oxidized and reduced) in SCC-61 and rSCC-61 cells was measured at 1 h after treatment with 2 Gy of ionizing radiation. Quantification is based on three biological replicates, and the respective p-values are $***p<0.001$ for total and oxidized glutathione (0 Gy and 2 Gy) and reduced glutathione (2 Gy); $**p=0.005$ for reduced glutathione (0 Gy). DCF, dichlorofluorescein; GSTpi, glutathione S-transferase pi; ROS, reactive oxygen species; SOD, superoxide dismutase. To see this illustration in color, the reader is referred to the web version of this article at www.liebertpub.com/ars

damage. As shown in Figure 7, there was a lower number of γH2AX foci formation in rSCC-61 compared with SCC-61 in response to radiation treatment, indicating decreased DNA damage in rSCC-61 compared with SCC-61 [Western blot analysis (Fig. 7A); Immunofluorescence analysis of γH2AX foci (Fig. 7B, C)]. This was further supported by the IPA analysis of the proteomic data using the function prediction tool, in which the fold change of a number of proteins listed in Supplementary Table S7 pointed toward reduced DNA damage in rSCC-61.

Relationship between ROS, lipid rafts, and the response to radiation and Erlotinib treatment

Another significant consequence of radiation-induced ROS is triggering the coalescence of lipid microdomains in the plasma membrane to form enlarged lipid rafts. Both resistance to radiation and increased sensitivity to EGFR inhibitors have been independently correlated to decreased lipid rafts and decreased localization of EGFR within these structures. The decreased basal and radiation-induced ROS in rSCC-61 coupled with the sevenfold upregulation of FASN in this cell line (Supplementary Table S3) led us to explore the potential differences in the lipid raft arrangements in SCC-61 and rSCC-61 cells. The cells were stained for lipid rafts and EGFR. Unlike rSCC-61, the SCC-61 cells showed increased lipid raft formation and EGFR co-localization within these structures in both control and radiated cells (Fig. 8A).

We then asked whether a decrease in the intracellular ROS in SCC-61 would influence the formation of lipid rafts and whether the disruption of lipid rafts would affect the response to Erlotinib or radiation. The SCC-61 cells were

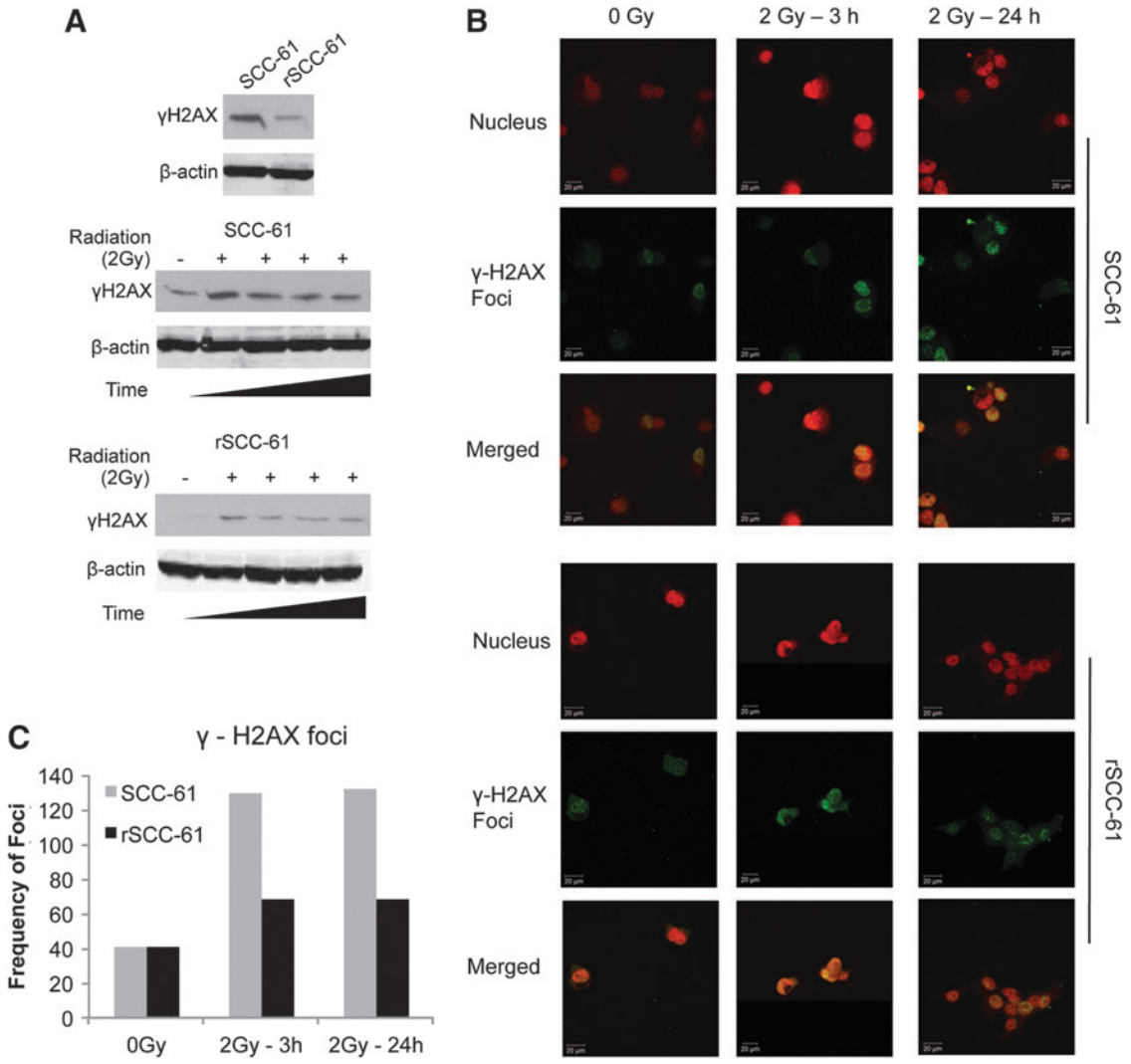

FIG. 7. Western blot and immunofluorescence analysis of γH2AX. (A) SCC-61 and rSCC-61 cells were irradiated with 2 Gy and lysed at different time intervals (0.5, 2, 6, and 24 h) followed by immunoblotting with γH2AX antibody. β-actin is used as a loading control. (Note: the SCC-61 and rSCC-61 samples were processed in a single 10-well SDS-PAGE gel. The image was separated to accommodate space available in the figure.) **(B)** and **(C)** Quantification of γH2AX foci in SCC-61 and rSCC-61 using immunofluorescence staining. Untreated cells and cells irradiated with 2 Gy were imaged using anti-γH2AX antibody (green) and Topro-3-iodide for nucleus (red). Frequency of foci was based on the monitoring of an average of 50 cells per experimental condition.

treated with polyethylene glycol-catalase, and the lipid rafts were stained with cholera toxin subunit B (Fig. 8B). A gradual disruption of lipid raft structures was observed on increasing catalase activity (2 and 20 U, respectively). The results were comparable with those obtained by the treatment of cells with a cholesterol extracting cyclodextrin MβCD and/or Lovastatin, an inhibitor of cholesterol biosynthesis (Fig. 8C) (14). Further experiments were performed to investigate the impact of lipid rafts in SCC-61 on the response to Erlotinib and radiation. As shown in Figure 8D and E, the disruption of lipid rafts increased the sensitivity of SCC-61 to Erlotinib and rendered the cells more resistant to radiation, a phenotype characteristic of rSCC-61.

Evaluation of redox balance in HNSCC clinical samples

Given the *in vitro* data showing a mechanistic connection between the control of ROS and resistance to radiation, we next investigated whether this has relevance *in vivo*. We have used the redox biotin-tagged probe BP1 [Fig. 9A, (44)] to investigate the protein oxidation as a marker of ROS in a set of HNSCC tumor samples. The criteria for tumor selection and grouping into the treatment ''responsive'' and ''resistant'' groups are presented in the ''Materials and Methods'' section. The control experiments showing the selectivity of BP1 for oxidized proteins and the lack of signal in the absence of BP1 are presented in Figure 9B. The quantification of BP1 staining in the radiation- and chemoradiation-resistant and -responsive HNSCC groups shows statistically significant differences in protein oxidation, providing initial validation of the *in vitro* findings (Fig. 9C).

Discussion

Surgery, radiation, and chemotherapy are the major modes of treatment for HNSCC, and resistance to radiation or chemotherapy poses significant problems in disease

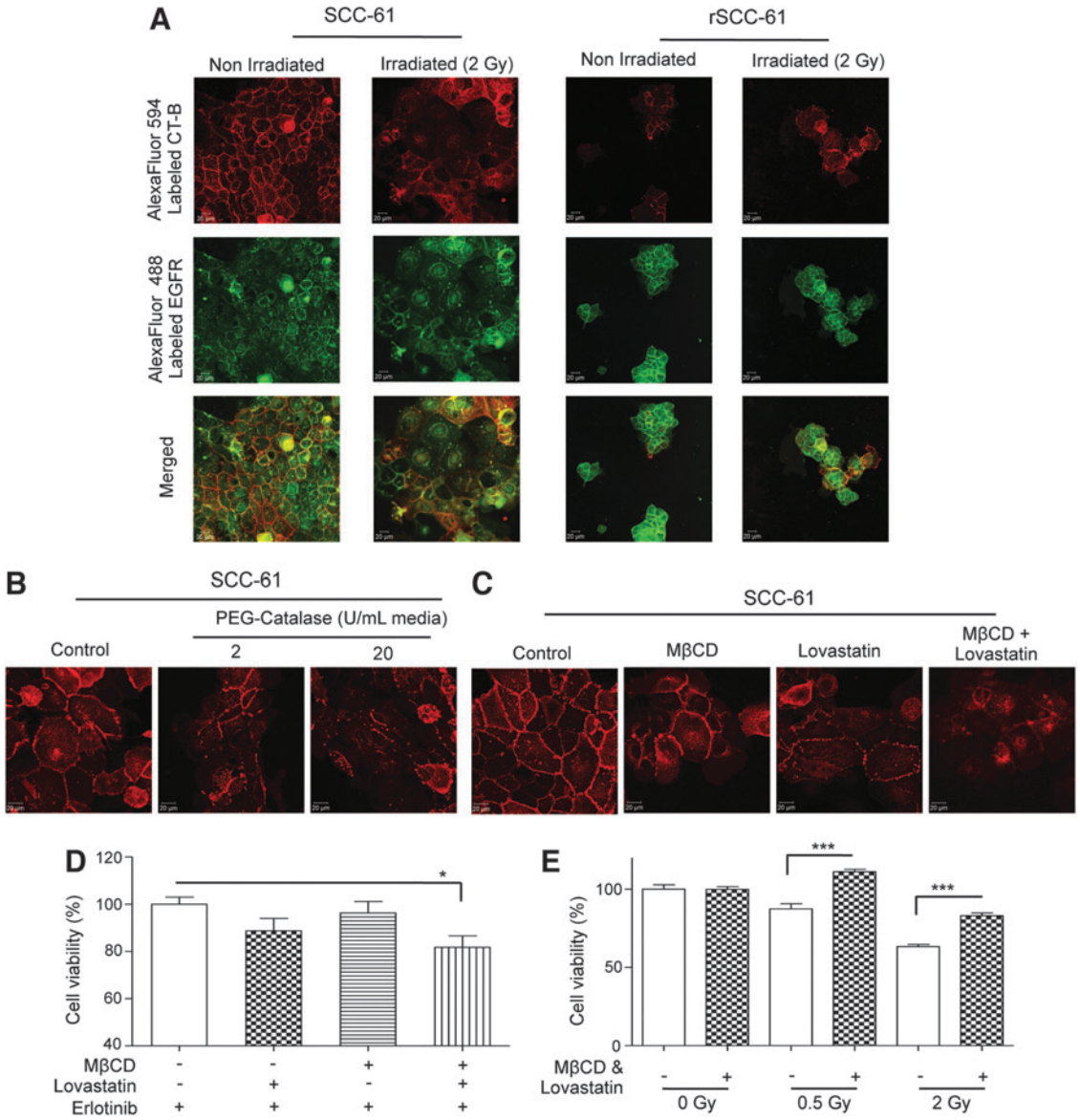

FIG. 8. Lipid rafts and response to radiation and EGFR inhibition. **(A)** Imaging of lipid rafts in SCC-61 and rSCC-61 cells. SCC-61 and rSCC-61 cells were either untreated or irradiated with 2 Gy followed by staining for confocal microscopy with cholera toxin subunit B (CT-B) conjugated to AlexaFluor594 (red) and EGFR antibody conjugated to AlexaFluor488 (green). The scale bars represent a distance of 20 μm. **(B)** The role of ROS in lipid raft formation in SCC-61. The SCC-61 cells were treated with 2 and 20 U of catalase and for 24 h followed by staining with AlexaFluor594 conjugated CT-B. A gradual decrease in the structural integrity of lipid rafts is observed. The scale bars represent a distance of 20 μm. **(C)** Inhibition of lipid rafts by MβCD and Lovastatin in SCC-61. The SCC-61 cells were treated for 24 h with 1 m*M* MβCD, 2 μ*M* Lovastatin or 1 m*M* MβCD plus 2 μ*M* Lovastatin and imaged using AlexaFluor594 conjugated CT-B. A decrease in the lipid rafts formation is observed under all treatment conditions. The scale bars represent a distance of 20 μm. **(D)** Inhibition of lipid rafts results in improved response to Erlotinib in SCC-61. After 24 h pretreatment of SCC-61 with MβCD, Lovastatin, or MβCD plus Lovastatin, the cells were treated with 2 μ*M* Erlotinib for 48 h, The cell viability was determined using the MTT assay. An increased response to Erlotinib was observed under all treatment conditions and achieved statistical significance under combined MβCD and Lovastatin treatment ($*p = 0.0189$, $n = 4$). **(E)** Inhibition of lipid rafts results in decreased response to radiation in SCC-61. After 24 h pretreatment of SCC-61 with MβCD plus Lovastatin, the cells were treated with 0.5 and 2 Gy radiation. After 48 h, the cell viability was determined using the MTT assay. A statistically significant increase in resistance to radiation was noted at both radiation doses in the MβCD and Lovastatin-treated cells relative to the untreated control (0.5 Gy: $***p < 0.001$; 2 Gy, $n = 4$: $***p < 0.001$, $n = 4$).

management. While the newer EGFR therapies show significant promise, only $\sim$10% of HNSCC tumors respond to Cetuximab; for example, despite the fact that more than 80% of these tumors have increased EGFR (9, 20). It is, therefore, highly important to identify the critical molecular features involved in response to radiation, chemotherapy, and targeted therapies. These would facilitate the discovery and validation of clinical biomarkers to predict the response to a particular treatment in HNSCC patients; to date, such biomarkers are not available in clinics.

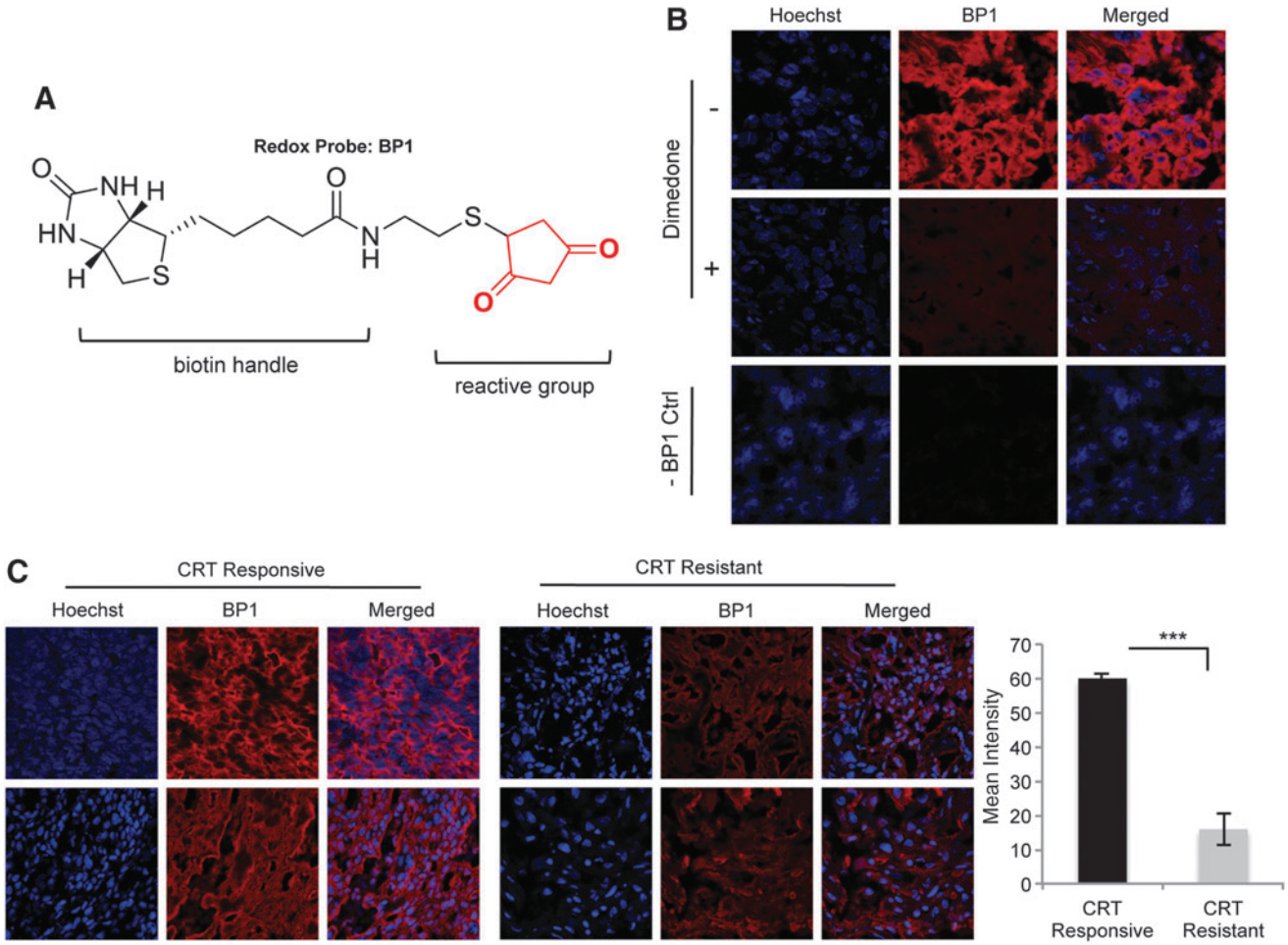

FIG. 9. Increased protein oxidation in clinical samples of radiation and chemoradiation-responsive HNSCC. (A) The chemical structure of the redox probe BP1. The structure highlights the 1,3- cyclopentanedione reactive group and the biotin tag that is used to detect labeled proteins. **(B)** Control experiments. The control experiments address the specificity of the probe toward oxidized proteins and the lack of signal in the absence of probes. **(C)** Representative staining of two tissue samples from the treatment-responsive and treatment-resistant groups. The tissues were treated with BP1 and visualized using Streptavidin-linked AlexaFluor594. Hoechst was used as a counterstain for the nuclei. The quantification of BP1 staining in the five samples/group was performed using ImageJ (***$p < 0.001$, $n = 5$). CRT, radiation or chemoradiation treatment; HNSCC, head and neck squamous cell cancer.

Our studies show a complex mechanistic connection between cellular phenotype (epithelial/mesenchymal), extracellular environment (pH, ROS), and the response to radiation or Erlotinib in HNSCC cells. A summary of the results is presented in Figure 10A and B, and the mechanistic connections are further discussed next.

Reversible epithelial-to-mesenchymal transition and response to radiation and Erlotinib

The epithelial-to-mesenchymal transition (EMT) has gained attention because of its role in the acquisition of cancer stem cell properties. In this process, the cells undergo cytoskeletal remodeling, loss of E-cadherin, and switch from keratin to vimentin-type intermediate filaments. The HNSCC tumors have been traditionally classified as mesenchymal characterized by loss of keratin and a substantial increase in vimentin (31). More recent studies, however, demonstrate the presence of both mesenchymal and epithelial cells in advanced-stage HNSCC tumors (5). There is extensive evidence that connects the epithelial or mesenchymal phenotype to the response to radiation, chemotherapy, or EGFR inhibitors. Examples include (i) the EMT transition was proposed to be responsible for the modest response of HNSCC tumors to small-molecule EGFR inhibitors such as Gefitinib (Iressa) and Erlotinib (Tarceva) (16); (ii) the increased keratin—a hallmark of epithelial phenotype—was correlated to resistance to DNA-damaging drugs (2, 12); (iii) in a study involving patients with advanced HNSCC, the non-keratinizing HNSCC responded better to combined radiation and chemotherapy than the tumors that expressed keratin (15, 36). These observations are consistent with the properties of the rSCC-61 cells described here. The upregulation of keratins, periplakin, and E-cadherin in rSCC-61, the decrease in vimentin, and the decreased migration in rSCC-61 are the main results that support the transition from a mesenchymal phenotype in SCC-61 to an epithelial phenotype in rSCC-61. This conclusion is also supported mechanistically by the quantitative proteomics analysis that showed down-regulation of functional pathways involved in migration and

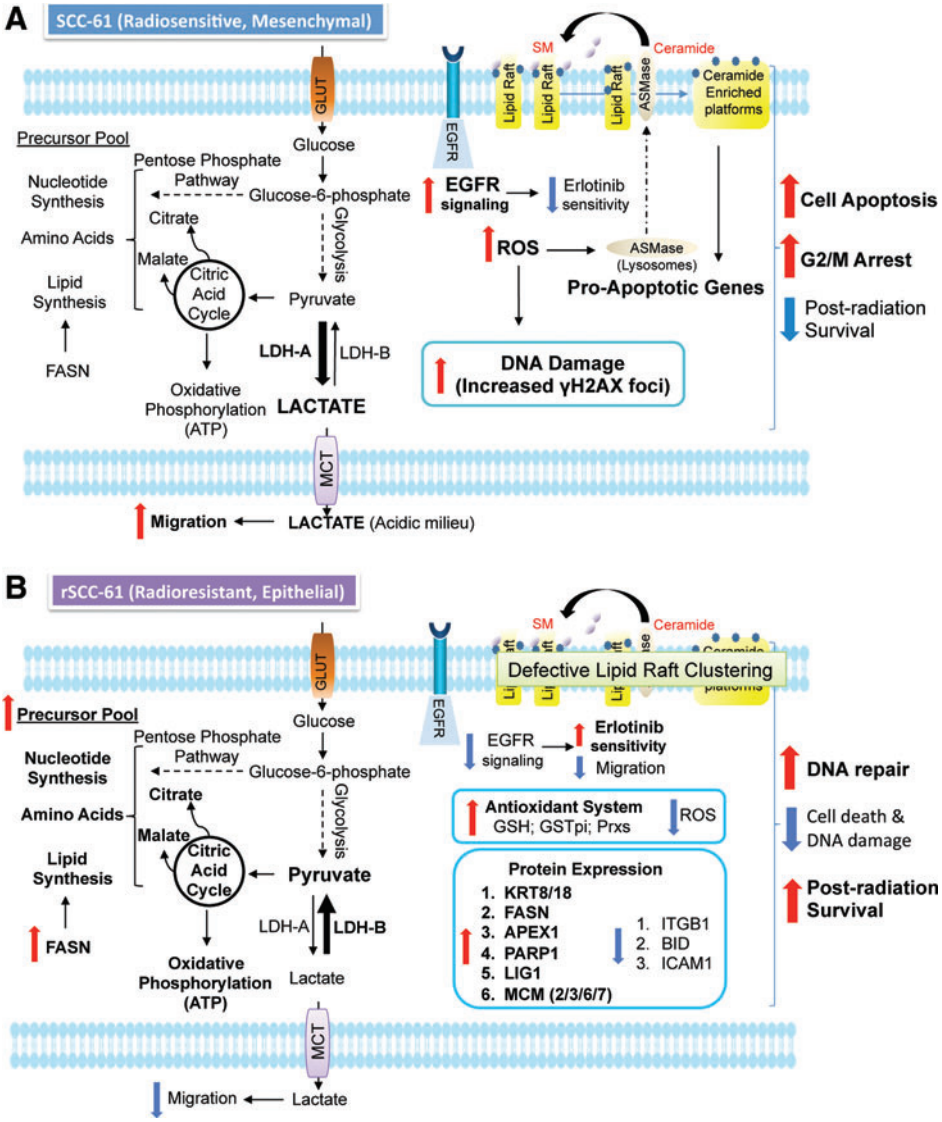

FIG. 10. Mechanistic model of radiation response in head and neck cancer. (A) Radiation-sensitive SCC-61 and **(B)** Radiation-resistant rSCC-61. SM, sphingomyelin; GLUT, glucose transporter; FASN, fatty acid synthase; LDH, lactate dehydrogenase (A or B); MCT, monocarboxylate transporter. To see this illustration in color, the reader is referred to the web version of this article at www.liebertpub.com/ars

cell morphology in rSCC-61 such as the ECM-receptor interaction, actin cytoskeleton regulation, and focal adhesion signaling. While the response of SCC-61 and rSCC-61 to radiation and Erlotinib is in accordance with the studies described earlier, the mechanisms involved are complex. We discuss next a potential network that may connect the cellular phenotype to the observed response to radiation and Erlotinib.

EGFR phosphorylation, ROS, lipid rafts, and response to radiation and Erlotinib

Observations from Figure 1F show that despite increased total phosphoprotein content in rSCC-61, there is significant downregulation of EGFR signaling in rSCC-61. The decreased phosphorylation of EGFR in rSCC-61 cells has two major consequences: (i) It results in reduced phosphorylation of downstream signaling proteins such as Akt, and the inhibition of Akt was previously shown to induce mesenchymal-to-epithelial transition in HNSCC cells (22); downregulation of Akt in rSCC-61 is further enforced by upregulation of PTEN, a negative regulator of Akt, in this cell line (Fig. 6B). (ii) Decreased phosphorylation of EGFR, along with the upregulation of antioxidant proteins, contributes to lower intracellular ROS through mechanisms that may involve decreased activation of NADPH oxidase and decreased glycolysis/mitochondrial electron transport chain, two major sources of ROS.

The regulation of redox microenvironment in rSCC-61 is important to explain both the resistance to radiation and the sensitivity to Erlotinib in rSCC-61. The Western blot analysis of γH2AX indicates reduced DNA damage in rSCC-61, and the cell cycle analysis shows reduced G2/M arrest with 2 Gy radiation in rSCC-61. Another contributing factor to reduced DNA damage with radiation results from upregulation of proteins involved in base-excision repair and DNA replication pathways shown by the proteomics data. In addition, both resistance to radiation and increased sensitivity to EGFR-inhibitors have been independently correlated to impaired structural rearrangement and formation of lipid rafts. Lipid rafts are a hub for the amplification of receptor signaling, including death receptor signaling, and are regulated by ROS—increased ROS have been linked to increased lipid raft formation (35, 38, 50). Our data show decreased ROS in

rSCC-61 and increased FASN in these cells. FASN is the main enzyme for synthesis of palmitate and lipogenesis, and its upregulation has been linked to resistance to chemotherapy and radiation (34, 53). FASN inhibition was also proposed to contribute to increased levels of ceramide, a major component of lipid rafts (4). The studies described here show lower lipid staining at the cell membrane in rSCC-61, which may contribute to the increased cell survival and sensitivity to EGFR inhibitors. Indeed, the disruption of lipid rafts in SCC-61 resulted in gain of resistance to radiation and improved sensitivity to Erlotinib. The increased sensitivity of rSCC-61 to Erlotinib is contrary to previous studies which show that cells resistant to EGFR-targeted inhibitors are cross-resistant to ionizing radiation (6, 17). Our results show that the connection between the resistance to radiation and EGFR inhibitors is not bidirectional and emphasizes the significance of adding targeted therapies to radiation or chemotherapy for improving clinical response to treatment. The analysis of protein redox status in clinical samples shows a clear difference between tumors that responded well to radiation and chemoradiation treatment and tumors which did not respond to treatment. This provides the necessary justification for further exploring protein oxidation as a potential biomarker of response to radiation and chemoradiation treatment.

In conclusion, we generated a matched model of radiation resistance in HNSCC that shows increased sensitivity to EGFR inhibition by Erlotinib. Cumulatively, quantitative proteomics, computational, and mechanistic investigations of this system show a convergence of signaling and metabolism networks to elicit protection against ionizing radiation. In some cases, such as the system described here, the acquired resistance to radiation can be accompanied by phenotypic changes or altered sensitivity to other treatments (*e.g.,* targeted inhibitors). The preliminary analysis of clinical samples using newly developed chemical probes for protein oxidation is consistent with the *in vitro* findings. Prospective clinical studies are ongoing and will address the predictive value of the potential biomarkers of response identified by the studies described here. These include global protein redox status, FASN level, EGFR phosphorylation, and tumor epithelial–mesenchymal composition.

Materials and Methods

Reagents and details of standard methods used in the study are included in the ''Supplementary Materials and Methods'' section

Cell culture and radiation treatment

All cells used in this study were cultured in the DMEM/F12 medium that was supplemented with 10% fetal bovine serum (FBS; Invitrogen) at 37°C and 5% CO_2. The head and neck cancer cell line SCC-61 was kindly provided by Ezra Cohen, Department of Medicine, University of Chicago. Fresh medium was added to cultured cells every 2 days. Subconfluent cells ($\sim$60%–80% confluency) were subjected to radiation with different doses as indicated for each experiment. Radiation was performed using a 444 TBq 12,000 Ci self-shielded ^{137}Cesium (Cs) irradiator. Culture dishes were placed on a styrofoam insert within the chamber of the irradiator, such that the distance from the Cs source results in a homogenous dose distribution over the desired field with a dose rate of 392 rad/min. From the dose rate, the exposure time required to deliver the desired dose was calculated and input into the irradiator.

Establishment of the radiation-resistant rSCC-61 clone

The radiation-sensitive SCC-61 cells were irradiated using a 2 Gy radiation dose. After the radiation treatment, the cells were cultured, split 1:2, allowed to achieve 60% confluence, and then exposed to another cycle of 2 Gy radiation. This process was repeated for a cumulative total of 16 Gy. The resulting cell population was plated at a low density on soft agar, and single cell colonies were picked and expanded in culture. The studies here were focused on the clone R8E, called rSCC-61.

Stable isotope labeling of amino acids in cell culture

The SCC-61 and rSCC-61 cells were cultured in DMEM/F12 media containing the light and heavy isotopes of Lys and Arg, respectively, and supplemented with 10% dialyzed FBS and 200 mg/L proline to prevent the conversion of isotope-coded arginine to proline in cells (7, 40). The cells were passed in their respective media to achieve a minimum of 97% incorporation of the isotope labeled Lys and Arg. The cells were then lysed in modified RIPA buffer (50 m*M* Tris-HCl, pH 7.4; 1% NP40; 0.25% Sodium deoxycholate; 15 m*M* NaCl; 1 m*M* EDTA; 1 m*M* NaF; supplemented with Roche protease and phosphatase inhibitor tablets). Protein concentration was determined using the bicinchoninic acid (BCA) assay (Thermo Scientific). The SCC-61 and rSCC-61 lysates were then mixed in a 1:1 ratio, precipitated using chloroform/methanol to concentrate the sample, and resuspended in 0.1% SDS. The mixed lysates were resolved on 12% SDS-PAGE and stained with Coomassie Brilliant Blue (R-250). The entire lane was divided into 15 gel bands, which were then digested with trypsin following standard in-gel digestion protocols (1). The resulting tryptic peptides were analyzed on a nanoLC system that was coupled with a LTQ Orbitrap mass spectrometer. Peptide separation was performed on a Thermo Scientific Acclaim PepMap RSLC column (15 cm, 2 μm particle sizes, 100 Å pore sizes) with a flow rate of 300 nL/min and using a 65 min gradient of solutions A (0.05% formic acid in water) and B (80% acetonitrile, 20% water, 0.05% formic acid). The mass spectrometer was operated in the data-dependent mode. The first MS scan was acquired in the Orbitrap at 60,000 resolution (m/z 300–2000). The following MS/MS scans were collected in the ion trap for the top five most intense ions using collision-induced dissociation. The raw MS files were analyzed by Proteome Discoverer 1.2 software (Thermo Fisher Scientific) using MASCOT search engine and the UniProtKB human database. The results were filtered using a false discovery rate of 1%.

Pathway and network analysis

IPA software (www.ingenuity.com) was used to identify significantly over-represented pathways and cellular functions in the list of identified proteins. The rSCC-61/SCC-61 proteomics data were imported into IPA and filtered on 2-fold change before a core analysis was performed to identify the most significantly regulated proteins and associated cellular functions. Additional network associations were generated

with Cytoscape version 2.8.2 (47) using KEGG and HPRD databases. The Cytoscape plug-in BioNetBuilder version 2.0 (3) was used to obtain all KEGG interactions available for humans on December 16, 2011 using default settings, while the plug-in BisoGenet was used to mine all available human interactions present in the list from the HPRD database on January 10, 2012. Network annotation analysis was performed on the lists of UniProt accessions by representing the proteins present in the KEGG and HPRD networks. Both lists were independently analyzed in the tools provided by the DAVID (23, 24). To determine what types of biological functions were over-represented in each network, the Annotation Clustering tool was used to analyze each list of proteins where only GO_FAT terms were selected for analysis and all other options remained at their default setting. Results were filtered for annotation clusters that had an Enrichment Score of 1.3 or greater (equivalent to a *p*-value of 0.05 or less).

Analysis of clinical samples

Tissue samples. Previously collected and deidentified tumor samples ($n=10$, flash frozen) were obtained from the Tumor Tissue Core Laboratory at Wake Forest School of Medicine (IRB # 00022263). All patients signed consent forms to permit the use of tumor specimens for scientific, developmental technology, research, and education purposes. Each of these 10 samples were squamous cell carcinomas of the base of tongue. Each patient had radiation as a component of upfront definitive treatment, whether it was radiation, chemoradiation, or surgery followed by radiation or chemoradiation. Treatment-responsive samples ($n=5$) were classified as those patients who had no evidence of any local or distant failure, or residual or persistent disease (such as noted in a neck dissection) within 1 year after completion of radiation. Of these five radiation sensitive samples, one patient underwent definitive chemoradiation, two patients underwent surgery with immediate adjuvant chemoradiation, and two patients underwent surgery with immediate adjuvant radiation alone. Treatment-resistant samples ($n=5$) were those who were found to have biopsy proven residual or persistent disease within 1 year of completion of radiation. Of these five radiation-resistant samples, one patient underwent definitive radiation and the remaining four patients underwent definitive chemoradiation. The biotin-tagged redox probe BP1 was synthesized in our laboratory following the procedure previously published (44).

Cryosectioning of frozen tissue samples. The flash frozen tissue blocks were stored at $-80°C$ until the time of sectioning. Before sectioning the frozen tissue, blocks were transferred to a cryotome cryostat (*e.g.,* $-20°C$) and allowed to equilibrate to the temperature of the instrument. The tissue sections (8 μm thickness) were placed on poly-L-lysine-coated glass slides.

BP1 staining for protein oxidation. The tissue sections were fixed by immersing the slides of 4% paraformaldehyde in 0.1 *M* phosphate-buffered saline (PBS) for 20 min at room temperature followed by washing 5×5 min with 0.1 *M* PBS. After fixation, the samples were permeabilized and stained with BP1 (500 μM) in 0.01 *M*, pH 7.4 PBS containing 0.2% Triton X-100 (PBT) for a total of 80 min. After this incubation, the slides were washed 5×5 min with PBS and then incubated with Streptavidin-AlexaFluor594 (Red) (2 mg/ml; 1:100 dilution in PBT). The slides were washed with PBS followed by nuclear staining with Hoechst (1:10,000 in 0.01 *M*, pH 7.4 PBS). Two control experiments were performed: 1. Dimedone, a nontagged reagent for protein oxidation (1 m*M*, 1 h) was added as blocking reagent before the addition of BP1; and, 2: the same staining procedure was followed as described earlier but in the absence of BP1.

Image collection, processing, and data analysis. A Zeiss 510 or 710 confocal microscope was used for the collection of images as indicated for each study. For each tissue sample, the $40\times$ images were taken at a laser intensity setting of 1% for all samples. All fluorescent excitation and emitted light collection settings were carefully held constant between samples to facilitate equivalence for intensity comparisons. LSM image browser was used for processing the confocal images. The mean fluorescence intensity in sections stained for BP1 was quantified using ImageJ.

Statistical analysis

Statistical analysis (*t*-test, one-way analysis of variance) was based on a minimum of three biological replicates using SigmaPlot v. 12.0. Asterisks indicate statistically significant changes compared with untreated controls ($\alpha=0.05$, *p*-values of 0.01–0.05 [*], 0.001–0.01 [**], or <0.001 [***]).

Acknowledgments

Research reported in this article was supported by the National Cancer Institute of the National Institutes of Health under award number R01 CA136810 to C.M.F. The authors also acknowledge financial support from the Wake Forest School of Medicine (development funds to C.M.F. and TRADONC fellowship to B.C.). An NSF Major Research Instrumentation award supported purchase of the LSCM used to generate images for the clinical samples included in this article (MRI-0722926) within the WFU Microscopic Imaging Core Facility. The clinical samples were obtained from the Tumor Tissue Core Laboratory of the Wake Forest University Comprehensive Cancer Center (grant number P30 CA12197).

Author Disclosure Statement

The redox probe BP1 is manufactured in the laboratory of C.M.F. and distributed by KeraFast. No competing financial interests exist for any of the other authors.

References

1. Aitken A and Learmonth M. Protein identification by in-gel digestion and mass spectrometric analysis. *Mol Biotechnol* 20: 95–97, 2002.
2. Anderson JM, Heindl LM, Bauman PA, Ludi CW, Dalton WS, and Cress AE. Cytokeratin expression results in a drug-resistant phenotype to six different chemotherapeutic agents. *Clin Cancer Res* 2: 97–105, 1996.
3. Avila-Campillo I, Drew K, Lin J, Reiss DJ, and Bonneau R. BioNetBuilder: automatic integration of biological networks. *Bioinformatics* 23: 392–393, 2007.
4. Bandyopadhyay S, Zhan R, Wang Y, Pai SK, Hirota S, Hosobe S, Takano Y, Saito K, Furuta E, Iiizumi M, Mohinta S, Watabe M, Chalfant C, and Watabe K. Mechanism of apoptosis induced by the inhibition of fatty acid synthase in breast cancer cells. *Cancer Res* 66: 5934–5940, 2006.

5. Basu D, Montone KT, Wang LP, Gimotty PA, Hammond R, Diehl JA, Rustgi AK, Lee JT, Rasanen K, Weinstein GS, and Herlyn M. Detecting and targeting mesenchymal-like subpopulations within squamous cell carcinomas. *Cell Cycle* 10: 2008–2016, 2011.
6. Benavente S, Huang S, Armstrong EA, Chi A, Hsu KT, Wheeler DL, and Harari PM. Establishment and characterization of a model of acquired resistance to epidermal growth factor receptor targeting agents in human cancer cells. *Clin Cancer Res* 15: 1585–1592, 2009.
7. Bendall SC, Hughes C, Stewart MH, Doble B, Bhatia M, and Lajoie GA. Prevention of amino acid conversion in SILAC experiments with embryonic stem cells. *Mol Cell Proteomics* 7: 1587–1597, 2008.
8. Bentzen SM, Atasoy BM, Daley FM, Dische S, Richman PI, Saunders MI, Trott KR, and Wilson GD. Epidermal growth factor receptor expression in pretreatment biopsies from head and neck squamous cell carcinoma as a predictive factor for a benefit from accelerated radiation therapy in a randomized controlled trial. *J Clin Oncol* 23: 5560–5567, 2005.
9. Bonner JA, Harari PM, Giralt J, Azarnia N, Shin DM, Cohen RB, Jones CU, Sur R, Raben D, Jassem J, Ove R, Kies MS, Baselga J, Youssoufian H, Amellal N, Rowinsky EK, and Ang KK. Radiotherapy plus cetuximab for squamous-cell carcinoma of the head and neck. *N Engl J Med* 354: 567–578, 2006.
10. Bump EA and Brown JM. Role of glutathione in the radiation response of mammalian cells *in vitro* and *in vivo*. *Pharmacol Ther* 47: 117–136, 1990.
11. Cappuzzo F. Erlotinib in gliomas: should selection be based on EGFR and Akt analyses? *J Natl Cancer Institute* 97: 868–869, 2005.
12. Caulin C, Ware CF, Magin TM, and Oshima RG. Keratin-dependent, epithelial resistance to tumor necrosis factor-induced apoptosis. *J Cell Biol* 149: 17–22, 2000.
13. Chong CR and Janne PA. The quest to overcome resistance to EGFR-targeted therapies in cancer. *Nat Med* 19: 1389–1400, 2013.
14. Christian AE, Haynes MP, Phillips MC, and Rothblat GH. Use of cyclodextrins for manipulating cellular cholesterol content. *J Lipid Res* 38: 2264–2272, 1997.
15. Crissman JD, Pajak TF, Zarbo RJ, Marcial VA, and Al-Sarraf M. Improved response and survival to combined cisplatin and radiation in non-keratinizing squamous cell carcinomas of the head and neck. An RTOG study of 114 advanced stage tumors. *Cancer* 59: 1391–1397, 1987.
16. Frederick BA, Helfrich BA, Coldren CD, Zheng D, Chan D, Bunn PA, Jr., and Raben D. Epithelial to mesenchymal transition predicts gefitinib resistance in cell lines of head and neck squamous cell carcinoma and non-small cell lung carcinoma. *Mol Cancer Ther* 6: 1683–1691, 2007.
17. Gee JM and Nicholson RI. Expanding the therapeutic repertoire of epidermal growth factor receptor blockade: radiosensitization. *Breast Cancer Res* 5: 126–129, 2003.
18. Gupta SC, Hevia D, Patchva S, Park B, Koh W, and Aggarwal BB. Upsides and downsides of reactive oxygen species for cancer: the roles of reactive oxygen species in tumorigenesis, prevention, and therapy. *Antioxid Redox Signal* 16: 1295–1322, 2012.
19. Haas-Kogan DA, Prados MD, Tihan T, Eberhard DA, Jelluma N, Arvold ND, Baumber R, Lamborn KR, Kapadia A, Malec M, Berger MS, and Stokoe D. Epidermal growth factor receptor, protein kinase B/Akt, and glioma response to erlotinib. *J Natl Cancer Inst* 97: 880–887, 2005.
20. Harari PM and Huang S. Radiation combined with EGFR signal inhibitors: head and neck cancer focus. *Semin Radiat Oncol* 16: 38–44, 2006.
21. Hirschhaeuser F, Sattler UG, and Mueller-Klieser W. Lactate: a metabolic key player in cancer. *Cancer Res* 71: 6921–6925, 2011.
22. Hong KO, Kim JH, Hong JS, Yoon HJ, Lee JI, Hong SP, and Hong SD. Inhibition of Akt activity induces the mesenchymal-to-epithelial reverting transition with restoring E-cadherin expression in KB and KOSCC-25B oral squamous cell carcinoma cells. *J Exp Clin Cancer Res* 28: 28, 2009.
23. Huang da W, Sherman BT, and Lempicki RA. Bioinformatics enrichment tools: paths toward the comprehensive functional analysis of large gene lists. *Nucleic Acids Res* 37: 1–13, 2009.
24. Huang da W, Sherman BT, and Lempicki RA. Systematic and integrative analysis of large gene lists using DAVID bioinformatics resources. *Nat Protoc* 4: 44–57, 2009.
25. Irwin ME, Mueller KL, Bohin N, Ge Y, and Boerner JL. Lipid raft localization of EGFR alters the response of cancer cells to the EGFR tyrosine kinase inhibitor gefitinib. *J Cell Physiol* 226: 2316–2328, 2011.
26. Jemal A, Siegel R, Ward E, Murray T, Xu J, and Thun MJ. Cancer statistics, 2007. *CA Cancer J Clin* 57: 43–66, 2007.
27. Kanda R, Kawahara A, Watari K, Murakami Y, Sonoda K, Maeda M, Fujita H, Kage M, Uramoto H, Costa C, Kuwano M, and Ono M. Erlotinib resistance in lung cancer cells mediated by integrin beta1/Src/Akt-driven bypass signaling. *Cancer Res* 73: 6243–6253, 2013.
28. Kanehisa M and Goto S. KEGG: Kyoto encyclopedia of genes and genomes. *Nucleic Acids Res* 28: 27–30, 2000.
29. Kao YC, Lee SW, Lin LC, Chen LT, Hsing CH, Hsu HP, Huang HY, Shiue YL, Chen TJ, and Li CF. Fatty acid synthase overexpression confers an independent prognosticator and associates with radiation resistance in nasopharyngeal carcinoma. *Tumour Biol* 34: 759–768, 2013.
30. Khodarev NN, Beckett M, Labay E, Darga T, Roizman B, and Weichselbaum RR. STAT1 is overexpressed in tumors selected for radioresistance and confers protection from radiation in transduced sensitive cells. *Proc Natl Acad Sci U S A* 101: 1714–1719, 2004.
31. Klymkowsky MW and Savagner P. Epithelial-mesenchymal transition: a cancer researcher's conceptual friend and foe. *Am J Pathol* 174: 1588–1593, 2009.
32. Lee YS, Chang HW, Jeong JE, Lee SW, and Kim SY. Proteomic analysis of two head and neck cancer cell lines presenting different radiation sensitivity. *Acta Otolaryngol* 128: 86–92, 2008.
33. Li B, Zhang C, He F, Liu W, Yang Y, Liu H, Liu X, Wang J, Zhang L, Deng B, Gao F, Cui J, Liu C, and Cai J. GSK-3beta Inhibition Attenuates LPS-Induced Death but Aggravates Radiation-Induced Death via Down-Regulation of IL-6. *Cell Physiol Biochem* 32: 1720–1728, 2013.
34. Liu H, Liu Y, and Zhang JT. A new mechanism of drug resistance in breast cancer cells: fatty acid synthase overexpression-mediated palmitate overproduction. *Mol Cancer Ther* 7: 263–270, 2008.
35. Lu SP, Lin Feng MH, Huang HL, Huang YC, Tsou WI, and Lai MZ. Reactive oxygen species promote raft formation in T lymphocytes. *Free Radic Biol Med* 42: 936–944, 2007.
36. Marcial VA, Pajak TF, Mohiuddin M, Cooper JS, al Sarraf M, Mowry PA, Curran W, Crissman J, Rodriguez M,

and Velez-Garcia E. Concomitant cisplatin chemotherapy and radiotherapy in advanced mucosal squamous cell carcinoma of the head and neck. Long-term results of the Radiation Therapy Oncology Group study 81-17. *Cancer* 66: 1861–1868, 1990.
37. Mitchell JB and Russo A. The role of glutathione in radiation and drug induced cytotoxicity. *Br J Cancer Suppl* 8: 96–104, 1987.
38. Morgan MJ, Kim YS, and Liu Z. Lipid rafts and oxidative stress-induced cell death. *Antioxid Redox Signal* 9: 1471–1483, 2007.
39. Nijkamp MM, Span PN, Hoogsteen IJ, van der Kogel AJ, Kaanders JH, and Bussink J. Expression of E-cadherin and vimentin correlates with metastasis formation in head and neck squamous cell carcinoma patients. *Radiother Oncol* 99: 344–348, 2011.
40. Ong SE and Mann M. A practical recipe for stable isotope labeling by amino acids in cell culture (SILAC). *Nat Protoc* 1: 2650–2660, 2006.
41. Park SH, Chung YM, Lee YS, Kim HJ, Kim JS, Chae HZ, and Yoo YD. Antisense of human peroxiredoxin II enhances radiation-induced cell death. *Clin Cancer Res* 6: 4915–4920, 2000.
42. Parkins CS, Stratford MR, Dennis MF, Stubbs M, and Chaplin DJ. The relationship between extracellular lactate and tumour pH in a murine tumour model of ischaemia-reperfusion. *Br J Cancer* 75: 319–323, 1997.
43. Prasad TS, Kandasamy K, and Pandey A. Human Protein Reference Database and Human Proteinpedia as discovery tools for systems biology. *Methods Mol Biol* 577: 67–79, 2009.
44. Qian J, Klomsiri C, Wright MW, King SB, Tsang AW, Poole LB, and Furdui CM. Simple synthesis of 1,3-cyclopentanedione derived probes for labeling sulfenic acid proteins. *Chem Commun* 47: 9203–9205, 2011.
45. Quiet CA, Weichselbaum RR, and Grdina DJ. Variation in radiation sensitivity during the cell cycle of two human squamous cell carcinomas. *Int J Radiat Oncol Biol Phys* 20: 733–738, 1991.
46. Ramsamooj P, Kasid U, and Dritschilo A. Differential expression of proteins in radioresistant and radiosensitive human squamous carcinoma cells. *J Natl Cancer Inst* 84: 622–628, 1992.
47. Smoot ME, Ono K, Ruscheinski J, Wang PL, and Ideker T. Cytoscape 2.8: new features for data integration and network visualization. *Bioinformatics* 27: 431–432, 2011.
48. Thomas GJ, Lewis MP, Whawell SA, Russell A, Sheppard D, Hart IR, Speight PM, and Marshall JF. Expression of the alphavbeta6 integrin promotes migration and invasion in squamous carcinoma cells. *J Invest Dermatol* 117: 67–73, 2001.
49. Tilghman RW, Slack-Davis JK, Sergina N, Martin KH, Iwanicki M, Hershey ED, Beggs HE, Reichardt LF, and Parsons JT. Focal adhesion kinase is required for the spatial organization of the leading edge in migrating cells. *J Cell Sci* 118: 2613–2623, 2005.
50. Ushio-Fukai M. Localizing NADPH oxidase-derived ROS. *Sci STKE* 2006: re8, 2006.
51. Weichselbaum RR, Beckett MA, Vijayakumar S, Simon MA, Awan AM, Nachman J, Panje WR, Goldman ME, Tybor AG, Moran WJ, *et al.* Radiobiological characterization of head and neck and sarcoma cells derived from patients prior to radiotherapy. *Int J Radiat Oncol Biol Phys* 19: 313–319, 1990.
52. Weichselbaum RR, Dahlberg W, Beckett M, Karrison T, Miller D, Clark J, and Ervin TJ. Radiation-resistant and repair-proficient human tumor cells may be associated with radiotherapy failure in head- and neck-cancer patients. *Proc Natl Acad Sci U S A* 83: 2684–2688, 1986.
53. Yang Y, Liu H, Li Z, Zhao Z, Yip-Schneider M, Fan Q, Schmidt CM, Chiorean EG, Xie J, Cheng L, Chen JH, and Zhang JT. Role of fatty acid synthase in gemcitabine and radiation resistance of pancreatic cancers. *Int J Biochem Mol Biol* 2: 89–98, 2011.

Address correspondence to:
Dr. Cristina M. Furdui
Section on Molecular Medicine
Department of Internal Medicine
Wake Forest School of Medicine
Winston-Salem, NC 27157

E-mail: cfurdui@wakehealth.edu

Date of first submission to ARS Central, October 29, 2013; date of final revised submission, February 6, 2014; date of acceptance, March 4, 2014.

Abbreviations Used

BCA = bicinchoninic acid
DAVID = Database for Annotation, Visualization and Integrated Discovery
DCF = dichlorofluorescein
DUT = deoxyuridine 5′-triphosphate nucleotidohydrolase
ECM = extracellular matrix
EGF = epidermal growth factor
EGFR = epidermal growth factor receptor
EMT = epithelial-to-mesenchymal transition
FASN = fatty acid synthase
GST = glutathione S-transferase
HNSCC = head and neck squamous cell cancer
HPRD = Human Protein Reference Database
IPA = Ingenuity Pathway Analysis
KEGG = Kyoto Encyclopedia of Genes and Genomes
KOH = potassium hydroxide
LDH = lactate dehydrogenase
MET = mesenchymal-to-epithelial transition
MTT = 3-(4,5-dimethylthiazol-2-yl)-2, 5-diphenyltetrazolium bromide
MβCD = methyl-β-cyclodextrin
NCR = nucleus-to-cytoplasm ratio
PEG = polyethylene glycol
PRX = peroxiredoxins
ROS = reactive oxygen species
SILAC = stable isotope labeling with amino acids in cell culture
SOD = superoxide dismutase